Inorganic Chemistry

Article

Structural and Luminescent Properties of Micro- and Nanosized Particles of Lanthanide Terephthalate Coordination Polymers

Carole Daiguebonne,*,† Nicolas Kerbellec,† Olivier Guillou,† Jean-Claude Bünzli,*,‡ Frederic Gumy,‡ Laure Catala,§ Talal Mallah,§ Nathalie Audebrand,‖ Yves Gérault,† Kevin Bernot,† and Guillaume Calvez†

Sciences Chimiques de Rennes—Equipe, Matériaux Inorganiques, Chimie Douce et Réactivité UMR CNRS-INSA 6226, INSA, 20 Avenue des buttes de Coësmes, 35043 Rennes, France, École Polytechnique Fédérale de Lausanne, Laboratoire de Chimie Supramoléculaire des Lanthanides, BCH 1402, CH-1015 Lausanne, Suisse, Laboratoire de Chimie Inorganique, UMR CNRS 8613, Université de Paris-Sud, 91405 Orsay, France, and Sciences Chimiques de Rennes—Equipe, Matériaux Inorganiques, Chimie Douce et Réactivité UMR CNRS-UR1 6226, Université de Rennes 1, Avenue du Général Leclerc, 35042 Rennes, France.

Reaction in water between rare earth ions (Ln = Y, La−Tm, except Pm) and the sodium salt of terephthalic acid leads to a family of lanthanide-based coordination polymers of general formula $[Ln_2(C_8H_4O_4)_3(H_2O)_4]_n$ with Ln = La−Tm or Y. The isostructurality of the compounds with the previously reported Tb-containing polymer is ascertained on the basis of their X-ray powder diffraction diagrams. The coordination water molecules can be reversibly removed without destroying the crystal structure for compounds involving one of the lighter lanthanide ions (La−Eu). For compounds involving one of the heavier lanthanide ions (Tb−Tm) or yttrium, a structural change occurs during the drying process. X-ray diffraction data show this new anhydrous phase corresponding to the linking of pairs of Er(III) ions through μ-carboxylate bridges. Porosity profiles calculated for the anhydrous phases of Tb(III) and Er(III) show the presence of channels with very small sections. The luminescent properties of all the compounds have been recorded and the two most luminescent polymers, namely, the europium- and the terbium-containing ones, have been studied in more detail. Tb(III)-containing compounds display large quantum yields, up to 43%. Polyvinylpyrrolidone nanoparticles doped with $[Ln_2(C_8H_4O_4)_3(H_2O)_4]_n$ (Ln = Eu, Tb, Er) have also been synthesized and characterized. The encapsulation of the coordination polymers results in somewhat reduced luminescence intensities and lifetime, but the nanoparticles can be dispersed in water and remain unchanged in this medium for more than 20 h.

Introduction

There is currently an increasing interest in luminescent systems. Lanthanide monomeric complexes often exhibit intense luminescence and are potentially interesting for the design of luminescent materials and devices.[1–9] There is also a strong quest for luminescent nanocrystals because of specific applications such as electroluminescent devices,[10] integrated optics,[11] or biological labels.[12,13] Some lumines-

* To whom correspondence should be addressed. E-mail: Carole.daiguebonne@insa-rennes.fr (C.D.); jean-claude.bunzli@epfl.ch (J.-C.B.).
† Sciences Chimiques de Rennes—Equipe, Chimie Douce et Réactivité UMR CNRS-INSA 6226.
‡ École Polytechnique Fédérale de Lausanne, Laboratoire de Chimie Supramoléculaire des Lanthanides.
§ Laboratoire de Chimie Inorganique, Université de Paris-Sud.
‖ Sciences Chimiques de Rennes—Equipe, Chimie Douce et Réactivité UMR CNRS-UR1 6226.

(1) Bünzli, J-C. G.; Piguet, C. *Chem. Rev.* **2002**, *102*, 1897.
(2) Yang, J.; Yue, Q.; Li, G.-D.; Cao, J. J.; Li, G.-H.; Chen, J. S. *Inorg. Chem.* **2006**, *45*, 2857–2865.
(3) Kido, J.; Okamoto, Y. *Chem. Rev.* **2002**, *102*, 2357–2368.
(4) Evans, R. C.; Douglas, P.; Winscom, C. J. *Coord. Chem. Rev.* **2006**, *250*, 2093–2126.
(5) Comby S.; Bünzli J.-C. G. Lanthanide Near-Infrared Luminescence in Molecular Probes and Devices. In *Handook on the Physics and Chemistry of Rare Earths*; Gschneider, K. A., Bünzli, J.-C. G., Pecharsky, V. K., Eds.; Elsevier: Amsterdam, 2007In press.
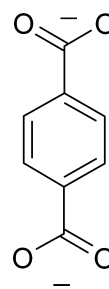(6) Bettancourt-Dias, A. *Inorg. Chem.* **2005**, *44*, 2734–2741.
(7) Wang, Z.; Jin, C. M.; Shao, T.; Li, Y. Z.; Zhang, K. L.; Zhang, H. T.; You, X. Z. *Inorg. Chem. Commun.* **2002**, *5*, 642–648.

cent nanocrystals have already been described.[13–15] To the best of our knowledge, despite numerous lanthanide-containing coordination polymers already reported,[16–26] none of them has been obtained in the form of nanosized luminescent particles. Moreover, most of the described coordination polymers have been obtained under hydrothermal conditions and very few lanthanide-containing coordination polymers have been obtained via soft chemistry routes.[27] However, the research on quantum dots has clearly shown that colloidal synthesis is a promising strategy to obtain luminescent nanocrystals suitable for potential applications. This synthetic strategy is based on a precipitation reaction in a medium containing a complexing agent able to limit the growth of the particles and to form a stabilizing shell at the surface thus preventing aggregation.[28–30]

Thanks to its rodlike topology, terephthalate presents low steric hindrance and leads, in association with lanthanide ions, to several different lanthanide-containing coordination polymers. Some of them have been obtained by hydrothermal methods[18,19,25,31,32] and the others by reaction in gel media.[21,33]

(8) Zhang, L. Z.; Gu, W.; Li, B.; Liu, X.; Liao, D. Z. *Inorg. Chem.* **2007**, *46*, 622–624.

(9) Yan, B.; Bai, Y.; Chen, Z. *J. Mol. Struct.* **2005**, *741*, 141–147.

(10) Colvin, V. L.; Schlamp, M. C.; Alivisatos, A. P. *Nature* **1994**, *370*, 354.

(11) Klimov, V. I.; Mikhailovsky, A. A.; Xu, S.; Holligsworth, J. A.; Leatherdale, C. A.; Eisler, H. J.; Bawendi, M. G. *Science* **2000**, *290*, 314.

(12) Bruchez, M. P.; Moronne, M.; Gin, P.; Weiss, S.; Alivisatos, A. P. *Science* **1998**, *281*, 2013.

(13) Nichkova, M.; Dosev, D.; Perron, R.; Gee, S. J.; Hammock, B. D.; Kennedy, I. M. *Anal. Bioanal. Chem.* **2006**, *384*, 631–637.

(14) Buissette, V.; Giaume, D.; Gacoin, T.; Boilot, J. P. *J. Mater. Chem.* **2006**, *16*, 529–539.

(15) Beaurepaire, E.; Buissette, V.; Sauviat, M.; Giaume, D.; Lahlil, K.; Mercuri, A.; Casanova, D.; Huignard A.; Martin, J. L.; Gacoin, T.; Boilot, J. P.; Alexandrou, A. *Nano Letters* **2004**, *4*, 2079–2083.

(16) Zhu, W.-H.; Wang, Z. M.; Gao, S. *Inorg. Chem.* **2007**, *46*, 1337–1342.

(17) Daiguebonne, C.; Guillou, O.; Gérault, Y.; Boubekeur, K. *J. Alloys Compd.* **2001**, *323–324*, 199–203.

(18) Reneike, T. M.; Eddaoudi, M.; Fehr, M.; Kelley, D.; Yaghi, O. M. *J. Am. Chem. Soc.* **1999**, *121*, 1651–1657.

(19) Reneike, T. M.; Eddaoudi, M.; O'Keeffe, M.; Yaghi, O. M. *Angew. Chem., Int. Ed.* **1999**, *38*, 2590–2594.

(20) Guillou, O.; Daiguebonne, C.; Camara, M.; Kerbellec, N. *Inorg. Chem.* **2006**, *45*, 8468–8470.

(21) Deluzet, A.; Maudez, W.; Daiguebonne, C.; Guillou, O. *Cryst. Growth Des.* **2003**, *3*, 475–479.

(22) Zhang, L. P.; Wan, Y. H.; Jin, L. P. *Polyhedron* **2003**, *22*, 981–987.

(23) Zheng, X.; Sun, C.; Lu, S.; Liao, F.; Gao, S.; Jin, L. *Eur. J. Inorg. Chem.* **2004**, *3262*, 3268.

(24) Candillas-Delgado, L.; Fabelo, O.; Ruiz-Perez, C.; Delgado, F. S.; Julve, M.; Hernandez-Molina, M.; Milagros Laz, M.; Lorenzo-luis, P. *Cryst. Growth Des.* **2006**, *6*, 87–93.

(25) Pan, L.; Zheng, N.; Wu, Y.-M.; Han, S.; Yang, R.; Huang, X.; Li, J. *Inorg. Chem.* **2001**, *40*, 828–830.

(26) Pan, L.; Adams, K. M.; Hernandez, H. E.; Wang, X.; Zheng, C.; Hattori, Y.; Kaneko, K. *J. Am. Chem. Soc.* **2003**, *125*, 3062–3067.

(27) Guillou O.; Daiguebonne C. Lanthanide ions containing coordination polymers. In *Handbook on the Physics and Chemistry of Rare Eaths*; Gschneider, K. A., Bünzli, J-C. G., Pecharsky, V. K., Eds.; Elsevier: Amsterdam, 2005; Vol. *34*, pp 359–404.

(28) Huignard, A.; Buissette, V.; Laurent, G.; Gacoin, T.; Boilot, J. P. *Chem. Mater.* **2002**, *14*, 2264.

(29) Catala, L.; Gacoin, T.; Boilot, J. P.; Rivière, E.; Paulsen, C.; Lhotel, E.; Mallah, T. *Adv. Mater.* **2003**, *15*, 826–829.

(30) Buissette, V.; Moreau, M.; Gacoin, T.; Boilot, J. P.; Chane-Ching, J.-Y.; Le Mercier, T. *Chem. Mater.* **2004**, *16*, 3767.

(31) Li, H.; Davis, C. E.; Groy, T. L.; Kelley, D.; Yaghi, O. M. *J. Am. Chem. Soc.* **1998**, *120*, 2186–2187.

Scheme 1. 1,4-Benzene-Dicarboxylate or Terephthalate Ligand (bdc^{2-})

In this paper, we describe the high yield synthesis of coordination polymers obtained by simple reaction in water between a lanthanide ion and terephthalate having the general formula $[Ln_2(C_8H_4O_4)_3(H_2O)_4]$ (Ln = Y, La−Lu, except Pm) where $(C_8H_4O_4)^{2-}$ stands for 1,4-benzene-dicarboxylate or terephthalate and is hereafter designated by bdc^{2-} (Scheme 1).

X-ray powder diffraction diagrams are analyzed to compare the structure of the reported compounds with the previously described structure of the Tb-containing compound.[18] The study is completed by thermal analyses and by an investigation of the photophysical properties. Furthermore, nanosized particles are also synthesized, and their optical properties are compared with those of the corresponding microcrystalline powders.

Experimental Section

Synthesis and Characterization of the Microcrystalline Powders of Hydrated Phases. Terephthalic acid was purchased from Acros Organics and used without further purification. Disodium terephthalate salt was prepared by addition of 2 equiv of sodium hydroxide to a suspension of terephthalic acid in deionized water. The obtained solution is then evaporated to dryness. The resulting solid is suspened in ethanol, stirred, and refluxed for one hour. After the mixture was filtered and dried on silica gel, a white powder of disodium 1,4-benzenedicarboxylate is collected in 90% yield. Elemental analysis of $C_8H_4O_4Na_2$ (MW = 210 g mol^{-1}) Calcd (Found): C 45.7% (45.5%); H 1.9% (2.0%); O 30.5% (30.5%); Na 21.9% (22.0%).

Hydrated lanthanide chlorides were prepared from the corresponding oxides according to literature methods.[34] Lanthanide oxides were purchased from STREM Chemicals and used without further purification.

Microcrystalline powders of the coordination polymers were obtained by mixing stoichiometric amounts of a lanthanide chloride in water with the disodium salt of terephthalic acid. Precipitation immediately occurred. The white precipitates were filtered and dried in air. The yields of the reactions are close to 100%. FT-IR spectra show the expected strong characteristic absorptions for the symmetric and asymmetric vibrations of benzene-dicarboxylate ligands

(32) Serre, C.; Millange, F.; Marrot, J.; Férey, G. *Chem. Mater.* **2002**, *14*, 2409–2415.

(33) Daiguebonne, C.; Kerbellec, N.; Bernot, K.; Gérault, Y.; Deluzet, A.; Guillou, O. *Inorg. Chem.* **2006**, *45*, 5399–5406.

(34) Desreux J. F. In *Lanthanide Probesin Life, Chemical and Earth Sciences*; Choppin, G. R., Bünzli, J.-C. G., Eds.; Elsevier: Amsterdam, 1989; p 43.

(35) Mighell, A. D.; Hubbard, C. R.; Stalick, J. K. *A Fortran Program for Crystallographic Data Evaluation*; Technical Note 1141; National Bureau of Standards: Gaithersburg, Maryland, 1980.

Scheme 2. Polyvinylpyrrolidone (PVP)
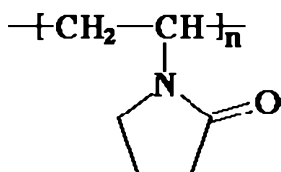
(1650–1550 and 1420–1335 cm^{-1}) and the coordinated water molecules (3460 cm^{-1}). They show no absorption band of any protonated ligand (1715–1680 cm^{-1}).

Single crystals have been obtained by slow diffusion in aqueous gel media of sodium terephthalate (Na$_2$bdc) and lanthanide chloride (LnCl$_3 \cdot n$H$_2$O, Ln = La, Ce, Er) solutions according to previously described procedures;[36,37] The three compounds were revealed to be isomorphous with [Tb$_2$(bdc)$_3$(H$_2$O)$_4$].[18] Their unit cell parameters are in perfect accordance with the refined unit cell parameters of the microcrystalline powders.

The microcrystalline powders obtained with Ln = Y, La−Tm, except Pm, have all been assumed to be isostructural to the previously described compound [Tb$_2$(bdc)$_3$(H$_2$O)$_4$]$_n$,[18,38] on the basis of their X-Ray powder diffraction diagrams. The extraction of the peak positions were carried out with the Socabim program PROFILE, which is a part of the DIFFRACT-AT software package supplied by Bruker AXS. The unit-cell parameters have been refined using the NBS*AIDS83 software package,[35] and they vary almost linearly with the ionic radius, as expected.

The granulometry of the microcrystalline compounds has been measured using a CILAS Laser Sizer 1180. All of the thirteen compounds display similar size distributions: 25% of the particles have a size of <0.3μm, 50% have a size that is between 0.3 and 1.4 μm, and the size of the remaining 25% ranges between from 1.4 to 9.0 μm (Figure S2). As one can notice, there is a great amount of particles around 50 nm. This can be related to the size of the crystallites that constitute the particles (see Figure 1).

For the microstructural analysis of [Tb$_2$(bdc)$_3$(H$_2$O)$_4$]$_n$, high-quality X-ray powder diffraction data were also collected at room temperature with a Siemens D500 diffractometer using monochromatic Cu Kα_1 radiation selected with an incident beam curved crystal germanium monochromator over the angular range of 20–67° (2θ), with steps of 0.015°, and 55 s counting time per step. Instrumental line profiles were obtained with the NIST standard reference material SRM660a LaB$_6$. For the whole pattern-fitting approach, the modeling of the instrumental profiles was carried out with the profile-fitting facility implemented in WinPLOTR.[39] The microstructure analysis was carried out from X-ray diffraction line-broadening analysis based on the whole pattern fitting technique by means of the program FULLPROF.[40] In this approach, the integral breadths of the individual Bragg reflections are derived from a pseudo-Voigt approximation to separate apparent volume-weighted size ϵ_β and microstrain e.

The powder data exhibit a small but significant diffraction line broadening compared to the instrumental broadening. The strong overlap of diffraction lines because of the low symmetry avoided

single-line analyses, and therefore, the microstructural analysis was carried out with the whole pattern-fitting technique by means of the program FULLPROF.[40] In the pattern matching, the Thomson−Cox−Hastings pseudo-Voigt function was selected to approximate the observed line profiles. The background was described with a linear interpolation between refined intensity points. The refinement involved the following parameters: 1 zero-point, 6 unit-cell parameters, 2 line asymmetry parameters, 14 parameters for the description of the background, and 2 crystallite size parameters. The final refinement converged to the residual factors R_P = 0.066 and R_{WP} = 0.091. The results were derived for isotropic line broadening with 55.5 nm for the apparent crystallite size and no residual strains. Because line broadening is isotropic, an average spherical shape can be assumed for the crystallites, and the corresponding average crystallite diameter ($4\epsilon_\beta/3$) is 74 nm.

The powders obtained with the heavier lanthanide ions, namely, ytterbium and lutetium, were found to have a general formula [Ln$_2$(bdc)$_3$(H$_2$O)$_8$]$\cdot$2H$_2$O and to be isostructural with [Er$_2$(bdc)$_3$(H$_2$O)$_8$]$\cdot$2H$_2$O.[33] These compounds will not be further described in this paper.

Synthesis and Characterization of the Microcrystalline Dehydrated Phases. Microcrystalline powders of compounds [Ln$_2$(bdc)$_3$-(H$_2$O)$_4$]$_n$ have all been dehydrated for 30 min in a furnace at 300 °C. The resulting dehydrated powders have then been analyzed by X-ray powder diffraction which revealed that dehydration leads to two families of compounds depending on the involved lanthanide ion: (i) for Ln = La−Eu, the crystal structure remains unchanged despite the removal of the coordination water molecules; (ii) on the other hand, dehydration modifies the crystal structure for heavier lanthanide ions (Tb−Tm).

The Gd-containing compound is borderline and loses most of its crystalline character upon dehydration. Therefore it has not been possible to attribute it unambiguously to one of these two families.

Synthesis and Characterization of the Nanosized Particles of [Ln$_2$(bdc)$_3$(H$_2$O)$_4$] with Ln = Eu, Tb, or Er. The synthesis consists in encapsulating nanoparticles into a polymer,[41,29] poly-vinylpyrrolidone, hereafter abbreviated PVP (see Scheme 2), purchased from Acros Organics and used without further purification.

An aqueous solution of lanthanide chloride (10^{-3} M) and PVP (10^{-1} M) was prepared and stirred vigorously. A solution of terephthalate disodium (1.5 × 10^{-3} M) was added, and the resulting solution was stirred for one hour. Propanone was added (propanone/water = 3:1 v/v), and precipitation immediately occurred. The mixture was centrifuged (8000 rpm for 10 min). The solid phase was then separated and dried under vacuum. This solid was a mixture of free PVP (PVP is insoluble in propanone and has been introduced in large excess) and of nanoparticles of [Ln$_2$(bdc)$_3$-(H$_2$O)$_4$] surrounded by coordinated PVP.

The FT-IR spectra display the expected strong characteristic absorptions for the symmetric and asymmetric vibrations of carboxylate functions (1386 and 1495 cm^{-1}) that do not exist in the spectrum of pure PVP. Elemental analysis and thermogravimetric analysis also confirm that the mixtures contain both [Ln$_2$(bdc)$_3$(H$_2$O)$_4$]$_n$ particles and PVP. The results are consistent for all the three samples and show that the lanthanide-containing particles constitute 17(1)% of the solid (in mass).[42] Elemental analysis of Tb$_2$C$_{24}$O$_{16}$H$_{20}$ and

(36) Daiguebonne, C.; Guillou, O.; Gérault, Y.; Boubekeur, K. *Recent Res. Dev. Inorg. Chem.* **2000**, *2*, 165–183.

(37) Daiguebonne, C.; Deluzet, A.; Camara, M.; Boubekeur, K.; Audebrand, N.; Gérault, Y.; Baux, C.; Guillou, O. *Cryst. Growth Des.* **2003**, *3*, 1015–1020.

(38) Tb$_2$(bdc)$_3$(H$_2$O)$_4$ crystallizes in the triclinic system, space group $P\bar{1}$ (No. 2). Its 8-fold coordination polyhedron can be described as a distorted dodecahedron.

(39) Roisnel, T.; Rodriguez-Carjaval, J. *Mater. Sci. Forum* **2000**, 118–123.

(40) Rodriguez-Carjaval, J.; Roisnel, T. *Newletter* **1998**, *20*, May-August.

(41) Uemura, T.; Kitagawa, S. *J. Am. Chem. Soc.* **2003**, *126*, 7814–7815.

(42) Samples have been heated in a platinum crucible at 900 °C under a flux of dioxygen until the organic part of the compound was destroyed. When the crucible contained only the lanthanide oxide it was possible to estimate the ratio Ln$_2$(bdc)$_3$(H$_2$O)$_4$/PVP. All measurements have been made three times to verify reproducibility.
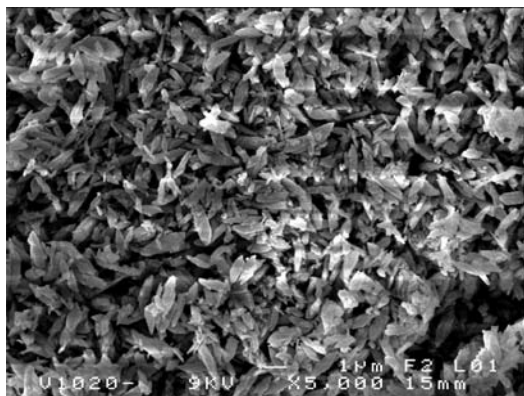
Figure 1. MEB photograph of a microcrystalline sample of $[La_2(bdc)_3(H_2O)_4]_n$.

$(C_6NOH_9)_n$ Calcd (found): Tb 6.0% (5.9%); C 59.3% (58.8%); H 7.1% (7.2%); N 10.4 (9.7%); O 17.2% (18.4%).

The presence of $[Ln_2(bdc)_3(H_2O)_4]$ particles has been unambiguously confirmed by X-ray diffraction diagrams which display the characteristic peaks of the corresponding bulk compounds. These diagrams have been difficult to record because of the presence of an amorphous polymer that produces a large diffusion band and because of the nanometric character of the lanthanide containing particles leading to a large broadening of the diffraction peaks. Finally, the nanometric character of the particles has been estimated using a Zetasizer Nano ZS (Malvern Instrument) and confirmed by STEM measurements. The size of the encapsulated particles lie in the range of 10–20 nm depending on the lanthanide ion and on the synthesis parameters.

The nanoparticles with $[Ln_2(bdc)_3(H_2O)_4]_n$ (Ln = Eu, Tb, Er) can be dispersed in highly polar solvents such as water, DMSO, or methanol. A typical STEM photograph of some dispersed Tb-containing nanoparticles is reproduced in Figure 2. The size of the dispersed particles is 3–5 nm.

X-ray Powder Diffraction. Most diagrams have been collected using a Panalytical X'Pert Pro diffractometer with an X'celerator detector. The typical recording conditions were 40 kV, 40 mA for Cu Kα (λ = 1.5418 Å); the diagrams were recorded in θ/θ mode in 60 min between 5° and 75° (8378 measurements) with a step size of 0.0084° in 2θ and a scan time of 50 s. The calculated patterns were produced using the Powdercell and WinPLOTR software programs.[39] The diagrams of the encapsulated nanoparticles have been recorded under different operating conditions: 40 kV, 40 mA for Cu Kα (λ = 1.5418 Å), the diagrams were recorded in θ/θ mode in 48 h between 5° and 75° (8378 measurements) with a step size of 0.0084° in 2θ and a scan time of 2500 s. Temperature-dependent X-ray powder diffraction experiments have been performed under nitrogen for $[Pr_2(bdc)_3(H_2O)_4]_n$ and $[Er_2(bdc)_3(H_2O)_4]_n$ between room temperature and 900 °C using a Panalytical PW1050/80 goniometer equipped with an Anton-Parr HTK 1200 furnace. The operating conditions were the following: 40 kV, 25 mA for Cu Kα (λ = 1.5418 Å). the diagrams were recorded in 2θ mode in 63 min between 5° and 70° (3750 measurements) with a step size of 0.02° in 2θ and a scan time of 1 s.

The high resolution X-ray powder diagram used for solving the structure of $[Er_2(bdc)_3]_n$ has been recorded with a Bruker AXS D5005 powder diffractometer using a diffracted-beam-graphite monochromator (Cu Kα$_{1,2}$) and equipped with an Anton Paar HTK1200 oven camera. High quality X-ray powder diffraction data for structure analysis were collected at 150 °C over the angular range of 7–80° (2θ) with a counting time of 80 s step^{-1} and a step length of 0.02° (2θ).

Thermal Analysis. Thermogravimetric and thermal differential analysis were performed in a platinum crucible under a nitrogen atmosphere between room temperature and 1000 °C with a heating rate of 5 °C·min^{-1} using a Perkin-Elmer Pyris-Diamon thermal analyzer.

Photophysical Measurements. Luminescence spectra of the hydrated microcrystalline powders were first recorded on a LS55 Perkin-Elmer luminescence spectrometer between 400 and 800 nm. An excitation wavelength of 312 nm has been chosen because it corresponds to a maximum of absorption of the terephthalate ligand.[43] The quantum yields have been determined by Wrighton's method[44] using an Oriel integration sphere. High-resolution spectra and lifetimes were measured on a previously described experimental setup.[45]

Results and Discussion

Structural and Thermal Aspects. The coordination polymers $[Ln_2(bdc)_3(H_2O)_4]_n$ (Ln = Y, La−Tm, except Pm) are isostructural with the $[Tb_2(bdc)_3(H_2O)_4]$ complex previously described.[18] The crystal structure consists of a three-dimensional molecular framework and presents no crystallization water molecules. The Ln(III) ions are 8-coordinate: they are bound to two oxygen atoms from coordinated water molecules and six oxygen atoms from carboxylato groups. Each Ln(III) ion is bound to six bdc^{2-} anions, and each anion is bound to four different Ln(III) ions (see Figure 3). The shortest intermetallic distances are summarized in Table 1.

Thermogravimetric analyses revealed that all the coordination polymers $[Ln_2(bdc)_3(H_2O)_4]_n$ present the same type of thermal behavior: The dehydration occurs in one step because there are only coordinated and no interstitial water molecules in the hydrated compounds. A dehydrated phase with general chemical formula $[Ln_2(bdc)_3]$ is obtained. This dehydrated phase is stable until decomposition of the coordination polymer leading to the corresponding lanthanide oxide. The characteristic dehydration and decomposition temperatures and the dehydration enthalpies measured for all the thirteen compounds studied are summarized in Figure 4.

It is noteworthy that the smaller the ionic radius of the involved lanthanide ion is, the smaller is the dehydration enthalpy, and that the lower is the dehydration temperature and the higher is the decomposition temperature. This is probably related to steric effect. Indeed, upon dehydration, the coordination number decreases and lanthanide ions exhibiting the smaller ionic radii accommodate more easily small coordination number than lanthanide ions with bigger ionic radii.

For compounds involving the lighter lanthanide ions (La−Eu) the crystal structure does not vary upon dehydration. This has been confirmed by temperature-dependent X-ray powder diffraction experiments between room temperature and 900 °C. On the other hand, for compounds involving the heavier lanthanide ions (Tb−Tm), the crystal

(43) Zheng, X. J.; Zheng, T. T.; Jin, L. P. *J. Mol. Struct.* **2005**, *740*, 31–35.
(44) Wrighton, M. S.; Ginley, D. S.; Morse, D. L. *J. Phys. Chem.* **1974**, *78*, 2229.
(45) Rodriguez-cortinas, R.; Avecilla, F.; Platas-Iglesias, C.; Imbert, D.; Bünzli, J.-C. G.; Blas, A.; Rodriguez-Blas, T. *Inorg. Chem.* **2002**, *41*, 5336–5349.
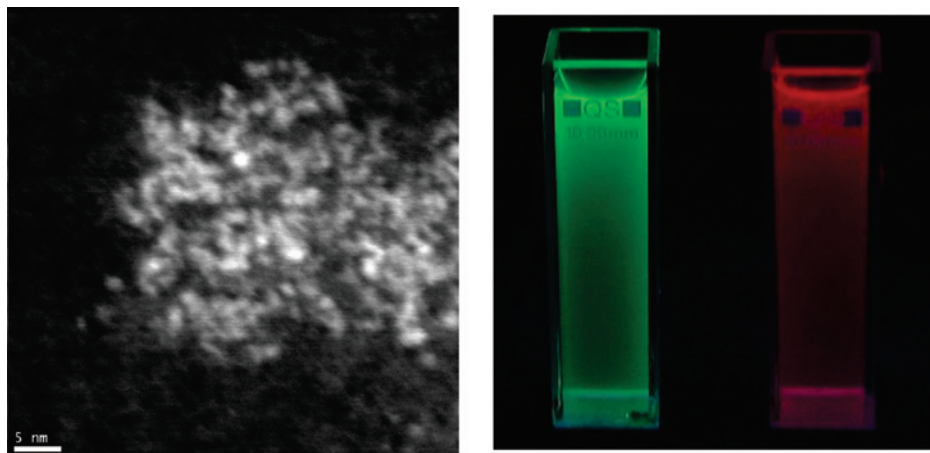
Figure 2. Left: STEM photograph of $[Tb_2(bdc)_3(H_2O)_4]_n$ nanoparticles. Right: Photograph under UV radiation (312 nm) of solutions containing dispersed nanoparticles doped with $[Tb_2(bdc)_3(H_2O)_4]_n$ (green) or $[Eu_2(bdc)_3(H_2O)_4]_n$ (red).
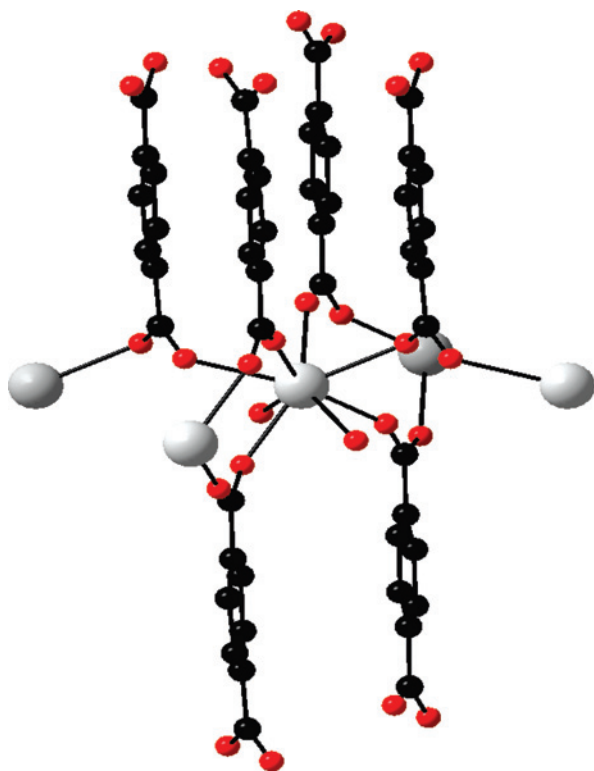
Figure 3. Projection view of an extended asymmetric unit of $[Tb_2(bdc)_3(H_2O)_4]_n$.

Table 1. Shortest Intermetallic Distances in $[Tb_2(bdc)_3(H_2O)_4]_n{}^a$

symmetry code	Tb–Tb distance (Å)
$1 + x, y, z$	6.142
$-1 - x, -1 - y, -1 - z$	5.093
$-1 - x, -1 - y, -z$	5.025
$-1 + x, y, z$	6.142
$-2 - x, -1 - y, -1 - z$	7.824
$-x, -1 - y, -1 - z$	8.131
$-x, -1 - y, -z$	7.938
$-2 - x, -1 - y, -z$	7.934
$2 + x, y, z$	12.284
$-2 + x, y, z$	12.284

^{a} All the distances are relative to the terbium atom with $(-0.50260, -0.48330, -0.24480)$ positional atomic coordinate that is with (x, y, z) symmetry code.

$98.832(5)°$, $\gamma = 107.279(5)°$, $V = 591$ Å^3, and $Z = 2$. These cell parameters, as well as the 3D-character of the structure (see Figure 6) are reasonable if compared with the similar features in the structure of the hydrated compound. As can be seen from Figure 6, the Er(III) ion is bound to seven oxygen atoms from carboxylate groups forming a distorted pentagonal bipyramid. Three carboxylato groups from three terephthalate ligands are coordinated in a bidentate fashion (coordination mode II, Scheme 3), while the seventh oxygen atom belongs to a carboxylato group that binds two metal ions via a μ_3-oxygen atom (coordination mode IV, Scheme 3).

As a comparison, each Er(III) ion is bound to six bridging carboxylato groups (coordination mode III) from six different terephthalate ligands in the crystal structure of the hydrated coordination polymer.

Therefore, the structural transition evidenced upon drying results in the linking of pairs of Er(III) ions through μ-carboxylato bridges. The Er–Er shortest distance is 3.5 Å (Table 2) in this dehydrated phase while it is 5.0 Å in the hydrated one.

In all cases, the anhydrous compound binds water reversibly when exposed to moisture, restoring the initial hydrated phase. This implies that both families of anhydrous compounds exhibit some porosity, at least for water. We have computed the porosity profiles of $[Ln_2(bdc)_3]_n$ (Ln = Tb,

structure is modified during the drying. All the $[Ln_2(bdc)_3]$ compounds with Ln = Tb−Tm have been assumed to be isostructural on the basis of their X-ray powder diffraction diagrams and a temperature-dependent X-ray diffraction experiment (using Panalytical PW1050/80 diffractometer) has been conducted between room temperature and 900 °C for Ln = Er (see Figure 5).

This experiment clearly indicates that a structural transition phase occurs upon drying, leading to a new anhydrous and stable phase. According to its X-ray powder diffraction diagram, the new compound crystallizes in the triclinic system, space group $P\bar{1}$ (No. 2) with $a = 10.1508(8)$ Å, $b = 8.9181(6)$ Å, $c = 7.4031(5)$ Å, $\alpha = 106.749(4)°$, $\beta =$

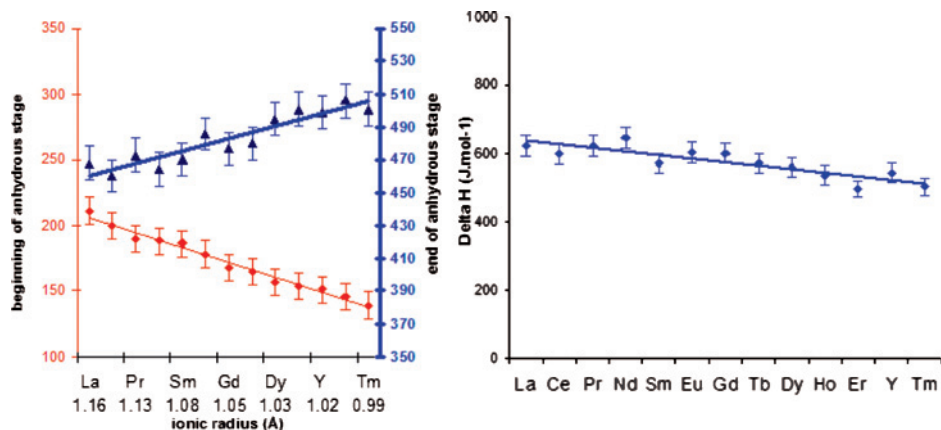**Figure 4.** Left: Plot of dehydration and decomposition temperatures versus lanthanide ionic radii for $[Ln_2(bdc)_3(H_2O)_4]_n$ (Ln = Y, La−Tm). Right: Plot of the corresponding dehydration enthalpies.

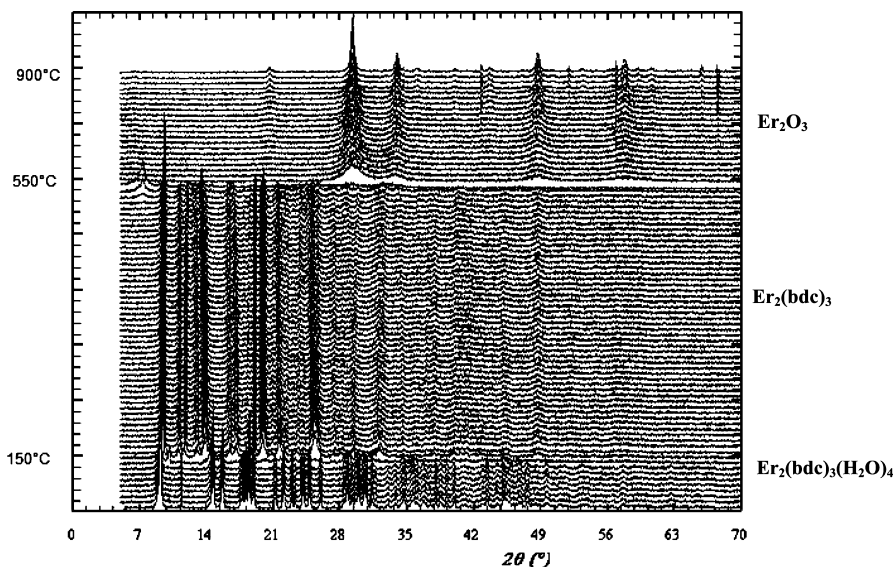**Figure 5.** Temperature-dependent X-ray diffraction plot for $[Er_2(bdc)_3(H_2O)_4]_n$.

Er) using previously described methods.[20,33,46] These calculations reveal that both crystal structures present very weak porosity. The channels diameters (1.8 Å) are too small for allowing adsorption of water (the kinetic diameter of a water molecule is 2.65 Å),[47,48] but rehydration is possible because the coordinatively unsaturated lanthanide ions inside the channels bind the incoming water molecules.

Photophysical Properties of the Hydrated and Dehydrated Phases. The three compounds containing Eu(III), Tb(III) or Dy(III) emit visible metal-centered luminescence (red, greenm and yellow, respectively), and the main features of these spectra are summarized in Figure 7. The main emission bands occur at 592 and 617 nm (Eu), 491 and 546 nm (Tb), and 481 and 575 nm (Dy).

The excitation spectrum of $[Eu_2(bdc)_3(H_2O)_4]$ has been recorded at room and low temperatures (10 K). They show both 4f−4f narrow peaks and a broadband from the bdc^{2-}

(46) Connolly, M. L. *Science* **1983**, *221*, 709–713.
(47) Albrecht, E.; Baum, G.; Bellunato, T.; Bressan, A.; Dall Torre, S.; D'Ambrosio, C.; Davenport, M.; Dragicevic, M.; Duarte Pinto, S.; Fauland, P.; Ilie, S.; Lenzen, G.; Pagano, P.; Piedigrossi, D.; Tessarotto, F.; Ullaland, O. *Nucl. Instrum. Methods Phys. Res.* **2003**, *A510*, 262–272.
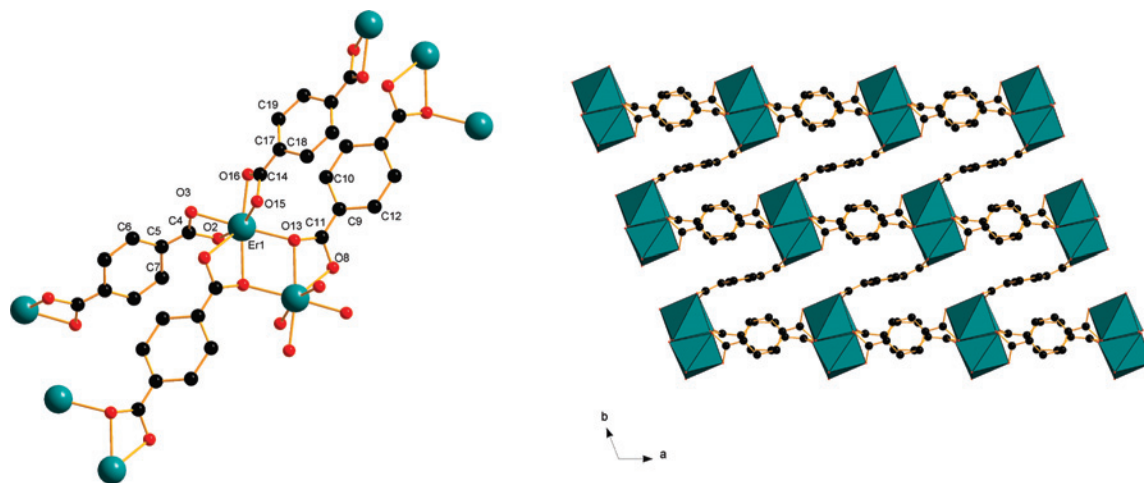
ligand, confirming sensitization of the Ln luminescence by the anion. However, the antenna effect may not be very large because the 4f−4f transitions dominate the spectra.

The high-resolution excitation spectrum of the Eu($^5D_0$ ← $^7F_0$) transition exhibits only one very sharp band (full width at half-height, fwhh = 4.5 cm^{-1}), pointing to the existence of a single and well-defined chemical environment for the metal ions (Figure 8). Its room temperature energy (17 767 cm^{-1}) can in principle be estimated from the nephelauxetic effect generated by the coordinated donor groups[49]

$$\tilde{\nu}(cm^{-1}, 295\ K) = 17\ 374 + \sum_i n_i \delta_i$$

where δ_i is the nephelauxetic effect of the donor group i and n_i is the number of coordinated donor groups. Taking $\delta_i(water) = -11.0$ cm^{-1} for an 8-coordinate Eu cation,[49] one can estimate $\delta_i(O-bdc) = -14.1$ cm^{-1} for a bridging carboxylate ion, as compared to -18.2 cm^{-1} for a nonbridging, monodentate carboxylate. Emission spectra of the Eu compound have been recorded under both broadband excitation and selective excitation at room and low temperatures. They are all very similar, which is consistent with a single

Figure 6. Left: Projection view along with numbering scheme of an extended asymmetric unit of $[Eu_2(bdc)_3]_n$. Right: Perspective view along the $\bar{c}$ axis of $[Er_2(bdc)_3]_n$. Er coordination polyhedra are drawn.

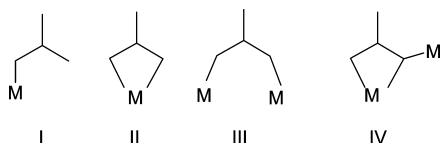**Scheme 3.** Some Coordination Modes Presented by the Carboxylato Groups

Table 2. Shortest Intermetallic Distances for $[Er_2(bdc)_3]_n{}^a$

symmetry code	Er–Er distance (Å)
$2 - x, 1 - y, 1 - z$	3.561
$2 - x, 1 - y, 2 - z$	5.445
$x, y, 1 + z$	7.369
$x, 1 + y, z$	8.904
$x, 1 + y, 1 + z$	9.815
$3 - x, 1 - y, 2 - z$	10.029
$1 + x, y, z$	10.142
$-1 + x, y, z$	10.142

^{a} All the distances are relative to the erbium atom with (0.99674, 0.35214, 0.62049) positional atomic coordinate that is with (x, y, z) symmetry code.

coordination site for europium ions. The emission spectrum is largely dominated by the $^5D_0 \rightarrow {}^7F_2$ transition at 616 nm with an intensity ratio I_2/I_1 with respect to the magnetic dipole transition $^5D_0 \rightarrow {}^7F_1$ equal to 6.9 at 295 K. The splitting of the $^5D_0 \rightarrow {}^7F_1$ transition in three components (589, 593, and 594 nm, corresponding to ligand-field sublevels at 301, 395, and 412 cm^{-1} for $^7F_1$) indicates that the Eu(III) ions lie in low-symmetry sites. However, the asymmetry of the splitting (94 and 17 cm^{-1}) allows one to interpret this transition in a pseudoaxial symmetry (singlet A and split doublet E) generating a negative B^2_0 crystal field parameter (~ -500 cm^{-1}).[50] We note that the observed splitting is similar to the one reported for a C_4-symmetric Eu complex with a cyclen derivative ($^7F_1$ sublevels at 300, 407, and 411 cm^{-1}).[51] The $^7F_1$ splitting determined for $[Eu_2(bdc)_3(H_2O)_4]$ is in agreement with its crystal structure in which each Eu(III) ion occupies the center of a slightly distorted square plane (see Table 3), yielding a metal ion environment with pseudo C_4 symmetry. The remaining $^5D_0 \rightarrow {}^7F_J$ transitions may also be related to the emission of an Eu centers with this symmetry (2, 3, and 6 transitions observed for $J = 2, 3,$

and, compared to 2, 3, and 5 allowed in C_4).

Dehydration of the Eu complex results in more complicated spectra, with the $^5D_0 \leftarrow {}^7F_0$ transition displaying at least two broad components (fwhh $\approx$ 8–10 cm^{-1}), a situation typical of the less well-defined metal environments found in polymeric systems.[34] A population analysis conducted on the $^5D_0 \rightarrow {}^7F_1$ transition shows the contribution of these two sites being about 50% each. Selective excitations on the $^5D_0 \rightarrow {}^7F_0$ transition reveal that one metal ion site generates three almost equally separated components (324, 359, 396 cm^{-1}), typical of a symmetry equal to or lower than C_2. The situation of the second site is different: if it seems to generate only two $^7F_1$ sublevels at 295 K (301 and 401 cm^{-1}), at least five components are evidenced at 10 K, revealing an intricate situation, again typical of a polymeric structure.

The excitation spectrum of $[Tb_2(bdc)_3(H_2O)_4]$ is largely dominated by the ligand bands, pointing to a good antenna effect. It is noteworthy that, upon dehydration, the 4f–4f transition disappears almost completely from the excitation spectrum. The emission spectra are not too informative; they are dominated by two multiplets centered around 491 and 546 nm attributed to the $^5D_4 \rightarrow {}^7F_6$ and $^5D_4 \rightarrow {}^7F_5$ transitions, respectively. Similar observations are made for the excitation spectra of $[Dy_2(bdc)_3(H_2O)_4]_n$. Both the hydrated and anhydrous complexes display intense emission from the $^4F_{9/2}$ level.

The luminescence decays of the Eu($^5D_0$) luminescence are single exponential functions when excitation is performed through the ligand bands, and there is no significant change between room and low temperature measurements. This indicates that the vibrational phenomena are not dominant in the nonradiative de-excitation process. Lifetimes of the excited levels are reported in Table 4, along with quantum yields determined with an integrating sphere under the same

(48) Breck D. W. *Zeolite Molecular Sieves*; John Wiley & Sons: New York, 1974.

(49) Frey, S. T.; Horrocks W.de, W., Jr. *Inorg. Chim. Acta* **1995**, *229*, 383.

(50) Görller-Walland C.; Binnemans K. In *Handbook on the Physics and Chemistry of Rare Earths*; Gschneider, K. A., Eyring, L., Eds.; Elsevier B.V.: Amsterdam, 1996.

(51) Zucchi, G.; Scopelliti, R.; Bünzli, J.-C. G. *J. Chem. Soc., Dalton Trans.* **2001**, 1975.
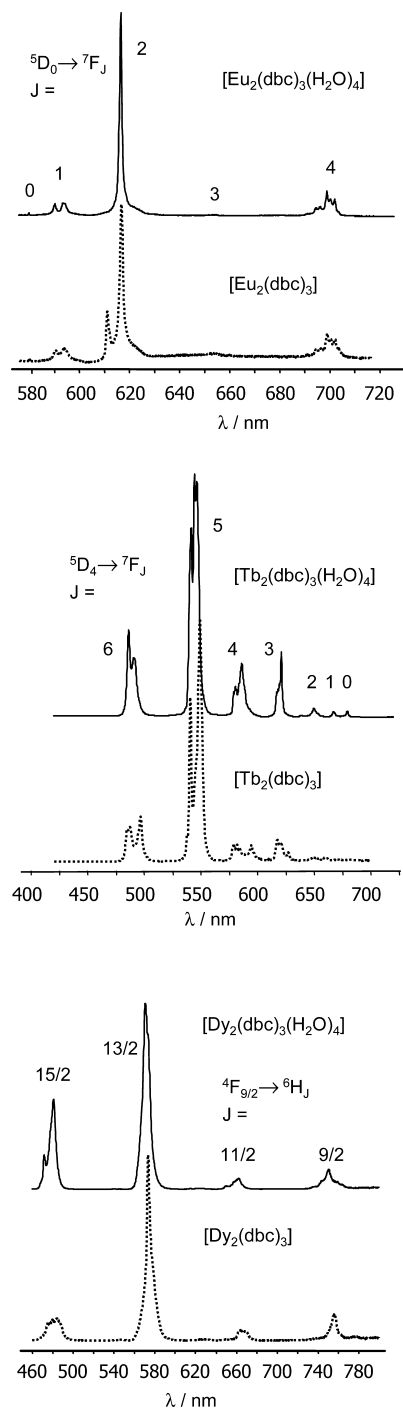
Figure 8. Eu($^5D_0 \leftarrow {}^7F_0$) excitation spectra for [Eu$_2$(bdc)$_3$(H$_2$O)$_4$]$_n$ recorded upon monitoring the $^5D_0 \rightarrow {}^7F_2$ transition.

Table 3. Selected Intermetallic Distances and Angles for [Eu$_2$(bdc)$_3$(H$_2$O)$_4$]$_n{}^a$

symmetry code	distance (Å)
−1−x, −1−y, −1−z	5.093
1+x, y, z	6.142
−1+x, y, z	6.142
−1−x, −1−y, −z	5.025

atom 1 symmetry code	atom 3 symmetry code	angle (deg)
−1 − x, −1 − y, −z	−1 + x, y, z	90.03
−1 + x, y, z	−1 − x, −1 − y, −1 − z	92.25
−1 − x, −1 − y, −1 − z	1 + x, y, z	87.75
1 + x, y, z	−1 − x, −1 − y, −z	89.97
1 + x, y, z	−1 + x, y, z	179.99
−1 − x, −1 − y, −z	−1 − x, −1 − y, −1 − z	172.37

^{a} The symmetry code of the considered central atom is (x, y, z).

Table 4. Quantum Yields, Φ (%), and Luminescent Lifetimes, τ (ms), at Room Temperature^a

sample	τ (ms)	Φ (%)
[Eu$_2$(bdc)$_3$(H$_2$O)$_4$]$_n$	0.47 ± 0.02	8.8 ± 0.7
[Eu$_2$(bdc)$_3$]$_n$	0.94 ± 0.01	12.4 ± 2.0
[Eu$_2$(bdc)$_3$(H$_2$O)$_4$]$_{\{nano\}}$	0.37 ± 0.01	7.4 ± 1.6
[Tb$_2$(bdc)$_3$(H$_2$O)$_4$]$_n$	1.04 ± 0.03	43.1 ± 1.6
[Tb$_2$(bdc)$_3$]$_n$	1.07 ± 0.02	26.4 ± 0.3
[Tb$_2$(bdc)$_3$(H$_2$O)$_4$]$_{\{nano\}}$	0.87 ± 0.05	26.3 ± 2.2
[Dy$_2$(bdc)$_3$(H$_2$O)$_4$]$_n$	1500 ± 20^b	c
[Dy$_2$(bdc)$_3$]$_n$	800 ± 10^b	c

^{a} The subscript {nano} stands for samples under the form of nanoparticles. ^{b} In ns. ^{c} Not determined.

Figure 7. Luminescent spectra recorded under broadband excitation (312 nm) at 295 K of solid samples of [Ln$_2$(bdc)$_3$(H$_2$O)$_4$]$_n$ and [Ln$_2$(bdc)$_3$]$_n$ coordination polymers with Ln = Eu, Tb, and Dy.

conditions. For the hydrated phase, the lifetime for Eu($^5D_0$) is in good agreement with the presence of two crystallization water molecules in the first coordination sphere (Table 4). After dehydration and upon selective excitation on the two evidenced sites, two different lifetimes are obtained, one corresponding to the lifetime of the hydrated species, 0.46 ± 0.04 ms and independent of temperature, and a much longer, temperature-dependent one ranging from 1.19 ± 0.03 ms at 295 K to 2.43 ± 0.03 ms at 10 K. The latter clearly reflects an Eu environment devoid of water molecule, while the shorter lifetime may be the result of short Eu−Eu
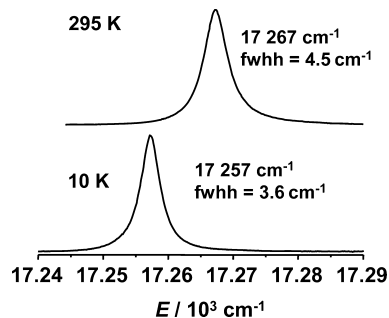
distances in the solid compound, resulting in energy migration between the sites (concentration quenching). The situation for the Tb($^5D_4$) luminescence is somewhat different in that both hydrated and dehydrated compounds present the same lifetime at room temperature, about 1 ms. Because the energy gap for Tb($^5D_4-{}^7F_0$) is larger than the corresponding one for Eu($^5D_0-{}^7F_6$), it is not unusual to have lifetimes ∼1 ms for a terbium ion bound to one or two water molecules. The temperature-dependence is, however, different for the two compounds: nil for the hydrated complex, while the $^5D_4$ lifetime of the anhydrous compound increases to 1.58 ± 0.02 ms at 10 K. This is clearly indicative of a temperature-dependent quenching mechanism which shortens the lifetime at room temperature. One explanation would be that a vibrationally assisted Tb−Tb energy-transfer mechanism is operative at higher temperature because the intermetallic distance revealed by the X-ray diffraction data for the anhydrous compound is quite short (3.5 vs 5 Å for the hydrated complex). The expected increase in the lifetime upon removal of the water molecules is therefore offset by

the new quenching mechanism taking place in the anhydrous compound. It is noteworthy that the lifetime of the $Dy(^4F_{9/2})$ level follows the same trend, becoming shorter in the anhydrous compound.

The quantum yields of the hydrated and dehydrated Eu(III) compounds measured under ligand excitation remain modest as expected from the excitation spectra. The 40% increase observed upon dehydration can be mainly related to the disappearance of the quenching mechanism by water molecules. Surprisingly, however, this is not the case for the Tb(III) compounds for which the quantum yield of the hydrated complex is significantly larger than the one of the anhydrous phase. This could be caused by two effects. First, the intermetallic distances in the anhydrous phase are quite shorter than in the hydrated phase, which could lead to a larger intermetallic de-excitation effect (concentration quenching, see above discussion on lifetime). A second explanation could be that the energy transfer between the bdc^{2-} anion and the Tb(III) cation is more efficient in the hydrated phase than in the dehydrated phase or that energy back transfer is less operative in the former case, as the blue shift of the ligand bands in the excitation spectrum suggests. The dehydrated sample has been exposed to water and indeed the initial value of $\Phi = 43\%$ was restored for this rehydrated sample.

Photophysical Properties of the Nanoparticle Encapsulated Complexes. The emission spectra of nanoparticles containing $[Ln_2(bdc)_3(H_2O)_4]_n$ (Ln = Eu, Tb) are very similar to the emission spectra recorded for bulk hydrated compounds. However, the $Eu(^5D_0)$ and $Tb(^5D_4)$ lifetimes (Table 4) are shorter than in both the corresponding hydrated and anhydrous parent compounds. Encapsulation of the complexes into the PVP nanoparticles therefore induces more nonradiative deactivation, and this is also reflected in the quantum yields. The quantum yield of the europium-containing nanoparticles is very close to the one of the hydrated bulk compound, while for Tb(III), it is close to the "anomalously" low quantum yield of the dehydrated phase, that is, significantly smaller than the one measured for the hydrated bulk compound. As the luminescent lifetime of the nanoparticles is also smaller, this difference could be attributed to an interaction with water in the second coordination sphere of the Tb(III) ion.

Finally, the stability of a nanoparticles dispersion in water has been checked by luminescence measurements. Encapsulated Tb-containing nanoparticles have been dispersed in bidistilled water. The dispersion presents a strong luminescence under UV radiation (254 nm). The emission

spectrum and the excited-state lifetime measurement have been performed hourly, and no change was observed even after 20 h.

Conclusion

In summary, we have reported the synthesis and the characterization of coordination polymers with general formula $[Ln_2(bdc)_3(H_2O)_4]_n$ with Ln = Y, La−Lu (except Pm). These compounds can be dehydrated, and the obtained anhydrous phases, which contain bridged pairs or Er(III) ions, reversibly bind water when exposed to a wet atmosphere. The coordination polymers with Ln = Eu, Tb, and Dy exhibit characteristic metal-centered luminescence. The largest quantum yields are obtained for the Tb(III) hydrated and anhydrous compounds, the value for the latter reaching 43%. Surprising difference in the photophysical properties of the anhydrous versus hydrated phases can be explained on the basis of structural changes between the two compounds, in particular, a shorter Ln−Ln distance in the anhydrous phases. Finally, to the best of our knowledge, we demonstrate for the first time that the luminescent $[Ln_2(bdc)_3(H_2O)_4]_n$ (Ln = Tb, Eu) coordination polymers can be encapsulated into PVP nanoparticles, while retaining most of their photophysical properties. The corresponding nanoparticle encapsulated complexes can be dispersed in water, which opens interesting perspectives for the use of these lanthanide-containing luminescent nano objects in materials sciences.

Supporting Information Available: Refined unit-cell parameters for $[Ln_2(dbc)_3(H_2O)_4]_n$ with Ln = Y, La−Tm. (Table S1), cell parameters versus involved rare earth ion for $[Ln_2(bdc)_3(H_2O)_4]_n$ (Ln = Y, La−Tm, except Pm) (Figure S1), size distribution of a microcrystalline sample of $[La_2(bdc)_3(H_2O)_4]_n$ (Figure S2), details concerning the structural characterization of $[Er_2(bdc)_3]_n$, and experimental and simulated X-ray powder diffraction diagrams of $[Er_2(bdc)_3]_n$ (Figure S3), thermal analysis curves for $[Nd_2(bdc)_3(H_2O)_4]_n$ (Figure S4), excitation spectra at 295 K of hydrated $[Ln_2(bdc)_3(H_2O)_4]_n$ and anhydrous $[Ln_2(bdc)_3]_n$ (Figure S5), and experimental X-ray powder diffraction diagrams of encapsulated $[Er_2(bdc)_3]_n$ nanoparticles (Figure S6). This material is available free of charge via the Internet at http://pubs.acs.org.

IC702325M